Significance of lognormal nanocrystal size distributions

R. Espiau de Lamaëstre[1,2] and H. Bernas[1,*]
[1]*CSNSM/CNRS, Université Paris Sud, 91405 Orsay Campus, France*
[2]*Fontainebleau Research Center, Corning SAS, 77210 Avon, France*
(Received 14 June 2005; revised manuscript received 14 November 2005; published 15 March 2006)

Metallic or semiconductor nanocrystals produced by very different techniques often display size distributions whose limiting shape (e.g., after long annealing times) is self-preserving and close to lognormal. We briefly survey the diverse microscopic mechanisms leading to this behavior, and present an experimental study of its inception in the case of semiconducting nanocrystals synthesized by ion implantation in silica. This example shows how the ultimate lognormal distribution is related to the system's memory loss of initial nucleation and growth processes.

DOI: 10.1103/PhysRevB.73.125317 PACS number(s): 64.75.+g, 81.07.−b, 05.40.−a, 85.40.Ry

I. INTRODUCTION

Many nanoscience studies involve attempts[1] to control nanocrystal average sizes and size distributions. Narrowing the latter is rarely easy. In specific cases, excellent results may be obtained by special chemical (notably colloidal[2] and sol-gel[3]) reactions. More often, reasonably narrow size distributions are the outcome of a carefully controlled nucleation and growth process. This implies an appropriate understanding of the process; typically, this is obtainable in a quasiequilibrium thermodynamics situation such as that of Ostwald ripening, where an analytical formulation of the long-term limit of the size distribution was obtained.[4,5] This is the so-called Lifshitz-Slyosov-Wagner (LSW) treatment,

$$f_{LSW}(R=r)=n_0\left(\frac{\langle R\rangle_0}{\langle R(t)\rangle}\right)^3\tilde{f}\left(\frac{r}{\langle R(t)\rangle}\right), \tag{1}$$

$$\tilde{f}(z)=3^4 2^{-5/3} e z^2 (z+3)^{-7/3}(3/2-z)^{-11/3}\exp\frac{1}{2z/3-1}, \tag{2}$$

where n_0 is some initial nanocrystal density of mean radius $\langle R\rangle_0$, and $\langle R(t)\rangle$ is the mean nanocrystal radius at time t.

In attempting[6] to broaden this approach experimentally, we encountered several instances in which the final size distribution was apparently lognormal as in Eq. (3), where μ is the geometric average and σ the geometric standard deviation:

$$f_{\text{lognormal}}(R=r)=\frac{1}{r\ln\sigma\sqrt{2\pi}}\exp\left(-\frac{(\ln r/\mu)^2}{2(\ln\sigma)^2}\right). \tag{3}$$

A search through the literature shows that this distribution is quite common[7] in many fields of physics and biophysics. To our knowledge, with the few exceptions referenced below it has rarely been discussed in the case of nanocluster synthesis in "hard" condensed matter, and there are no systematic experimental studies of its origin in that case. We report the results of our attempt to determine whether—and possibly how—physical information is obtainable on nanocrystal nucleation and growth from such a size distribution shape. Hopefully, this paper will stimulate further work in an area which may contribute greatly to nanocrystal size control.

The diversity of processes leading to lognormal size distributions is the first thing to emphasize. Aggregation of colloids[8] or of aerosols,[9] some crystallization processes,[10,11] some complex nucleation and growth processes,[12–15] all may lead to limiting size distributions that display apparently lognormal shapes. The fact that these processes involve very different microscopic mechanisms is clearly indicative of a very general property that we aimed to discern. This involved other questions. Where does the generality of lognormal shapes come from? Or conversely, what information on the physical process(es) occurring in an evolutionary system is contained in the lognormal distribution? For nanocrystals, if a nucleation and growth process leads to this limiting form of the size distribution, can the lognormal shape provide information on the differences between this process and that which leads to the LSW shape?

We encountered this problem in attempting to control the nucleation and growth of nanocrystals after ion implantation and/or irradiation. The main advantage of such techniques is to allow supersaturation of a solute in the host, but they also produce instabilities that lead away from equilibrium thermodynamics (radiation-enhanced or -induced diffusion, metastable compound formation, etc.). When pure metal clustering was involved, we found a case[16] in which nanocrystal synthesis led to a limiting size distribution corresponding almost exactly to the LSW prediction. On the other hand, many other ion-induced syntheses[12–15] gave rise to lognormal distributions. This paper reports a study of the latter observation's origin. For reference, Sec. II provides a brief survey of the phenomena leading to lognormal size distributions and precipitation in inhomogeneous systems. Section III reports a specific experimental study of a system produced by sequential implantation of two different elements in silica followed by postannealing. We show how a rather complex sequence (chemical solute-host interactions, ionic diffusion, nucleation and growth) lead to a well-defined lognormal size distribution as the limiting shape. In Sec. IV, based on the general approach of Binder,[17] we discuss the dynamics leading from the microscopic physical processes listed above to their translation in terms of a given size distribution. We show, in the case of nanocrystals grown after ion beam synthesis, that the multiplication of nucleation and

growth paths blurs the information contained in the size distribution. We relate this loss of information to the lognormal shape of the size distribution. In the perspective of the present work, ion beam synthesis has the advantage of multiplying—in a rather well-controlled way—interfering nucleation and growth mechanisms, but it should be noted that such effects are also encountered in many other growth situations, including coagulation.

Besides their interest as quantum systems, metallic or low-band-gap compound semiconductor nanocrystals in waveguide materials are of interest for photonics devices. The key parameters to be controlled are, besides the mean radius of the nanocrystals, precisely their size distribution and density. The results obtained here may therefore be of interest for both basic and applied physics.

II. GENERAL REMARKS

A. When are size distributions lognormal? A brief survey

Lognormal distributions are encountered in many areas of growth science. In the fields of cluster aggregation and coagulation, for example, considerable work has been done to link experimentally observed lognormal cluster size distributions to theoretical descriptions based on the initial work of Von Smoluchowski[18] regarding the coagulation process. He developed equations based on the following assumptions: (i) cluster formation starts from a population of monomers, and proceeds by successive binary collisions between clusters of any size; (ii) these binary collisions between species lead to *irreversible* coalescence, i.e., once formed, clusters can never become smaller. Thus, if n_k be the concentration of k-mers and K_{ij} the reaction rate constant between i- and j-mers, the time dependence of the k-mer concentration is given by

$$\frac{dn_l}{dt} = \frac{1}{2}\sum_{l'=1}^{l-1} K_{l',l-l'} n_{l'} n_{l-l'} - n_l \sum_{l'=1}^{\infty} K_{l',l'} n_{l'}. \tag{4}$$

In the literature, the K_{ij} are referred to as the kernels of the coagulation process. They describe the specific microscopic mechanism by which coagulation proceeds. For clusters diffusing in a solvent or a solid medium, depending on the medium density, coalescence occurs after collisions with both surrounding medium molecules and other clusters (Brownian regime), or with other clusters (ballistic regime). Thus, a cluster mean free path may be defined, involving a collision with another cluster, a monomer, or a solvent molecule. The amplitude of the mean free path depends on the nature of the medium, the solute volume fraction, etc.; it may also vary with the cluster size. As regards Brownian coagulation, theoretical developments by Friedlander *et al.*[19] showed that the asymptotic size distribution is self-preserving and close to a lognormal shape. In this regime, the mean free path of the cluster is smaller than their size, and growth can occur via cluster-cluster aggregation. These conclusions were supported by experimental evidence[20] as well as by numerical solutions of discrete kinetic equations.[21] Self-preserving distributions close to lognormal shapes were also observed for aggregation regimes with microscopic mechanisms differing from Brownian aggregation: e.g., steady-state shear[22] and ballistic or free molecular regimes[23] where the cluster mean free path was larger than its size. Asymptotic size distributions close to lognormal are also expected[24] in cases where the aggregates have fractal shapes. All these results were obtained for *closed* systems where an initially large population of particles or clusters coagulate, and they are independent of the initial state of the system.

Lognormal size distributions are also encountered after growth in *open* systems, such as in ultrafine particles synthesis by metal evaporation.[10,11] In the latter case, a growth-time model was developed to explain the lognormal shape of the size distribution:[25] evaporated metal particles form a layer above the bulk; a combination of particle diffusion and drift through this finite growth region leads to a lognormal growth-time probability density. Since the particle radius follows a power law of its growth duration, a lognormal distribution of growth times leads to a lognormal distribution of nanocrystal radii.

Lognormal size distributions have also been reported after nanocrystal formation after postannealing growth in Au-implanted silica,[12] GaN nanocrystals synthesis (by sequential Ga and N implantation and annealing) in dielectrics,[13] or postimplantation metal nanocrystal formation in Al.[14,15] In these examples, growth often occurs beyond the initial solute implantation range, and is usually limited by the diffusion of the implanted species. No link between the microscopic mechanisms and the observed size distribution shape was proposed and this paper aims at filling this gap. In Sec. III, we shall relate these results to the degree of information on the microscopic processes as growth proceeds: we show that they actually signal a loss of control over the growth process.

B. Precipitation in inhomogeneous systems

As discussed by Binder,[17] the asymptotic shape of a cluster size distribution is expected to depend on the nature of the physical system as well as on its growth mechanism. In the case of nanocrystal growth, it is interesting to contrast experimentally observed shapes with the shape expected from the LSW coarsening mechanism,[4,5] via condensation in a binary alloy solid phase, assuming a *uniform* average solute distribution. This leads to a well-defined asymmetric size distribution that has a tail on the small-precipitate side. The origin of size distribution broadening in the latter, as the cluster volume fraction increases, is the varying diffusional interaction between the solute concentration fields around the clusters.

When dealing with inhomogeneous systems, it is worthwhile introducing the screening length λ, which describes the concentration field interaction of neighboring clusters:

$$\lambda = \frac{1}{\sqrt{4\pi\langle R\rangle n}} \tag{5}$$

where n is the average cluster density and $\langle R\rangle$ their average radius. As growth occurs, the increase in average radius does not compensate the reduction in cluster density, so that the screening length progressively increases. The case where the solute distribution is *nonuniform*, as would be the case for an

ion-implanted sample with an implanted profile width Δ, was studied by Trinkaus[26] and Borodin.[27,28] If $\lambda \ll \Delta$, the local solute concentration nonuniformity may be neglected, and LSW-type growth occurs inside a (narrowed) implant profile. If $\lambda \gg \Delta$, on the other hand, solute diffusion occurs due to the concentration inhomogeneity, and clusters tend to dissolve by outdiffusion from the implant profile. Because of the increase in λ outdiffusion from the implanted layer should always be the main trend, at least as long as rather weak solute concentrations and quasiequilibrium thermodynamics are assumed, and interactions with radiation-induced defects are neglected. As a result, when the solute concentration is nonuniform the LSW equations must be modified to include loss of matter by diffusion (a quantity that now depends on the position in the sample). In other words, there is now a coupling between the system's evolution in real space (i.e., the cluster depth distribution) and in size space (the size distribution).

In the case of nanocrystal precipitation in glasses, the growth process may be complicated by complex solute-host chemical interactions that affect solute diffusion and precipitation thermodynamics. We have discussed these effects in some detail for lead chalcogenide nanocrystal growth in pure silica.[6,29] Here, we show how they systematically lead to a well-defined size distribution resembling a lognormal one.

III. EXPERIMENT

Our purpose was to set up a series of experiments in which we could deliberately relax one or another controlling factor in our samples, in order to determine whether this would ultimately bring the limiting shape of the size distribution to lognormal. All the samples in these experiments were synthesized by sequential ion implantation of Pb and chalcogens in pure silica at energies such that their initial concentration profiles overlapped. The conditions for sequential ion implantation and annealing were those of our previous work,[6,29,30] and are summarized in Table I. The anneals were performed in a quartz tube furnace under dry N_2 atmosphere, at temperatures ranging from 800 to 900 °C. Nanocluster identification, radius and density measurements were performed via transmission electron microscopy (TEM) on cross-sectional samples cut from the ion-implanted and annealed glasses, using methods detailed in Ref. 30. The TEM image treatment is summarized in the Appendix. In the following, we first studied the effect of allowing varying amplitudes of Pb and S diffusion by changing the annealing temperature or annealing time (at constant temperature). We then studied—by comparing results from samples implanted with different chalcogens—the effect of changing the chemical interactions of the implanted components in silica. Our previous work[6,30] revealed a rather strong relation between the implanted components' diffusion and their chemical interactions with the host or among themselves, so that the hierarchy of conditions controlling the systems' evolution is ambiguous. In spite of this ambiguity, quite different initial size distributions led to quasi-identical lognormal limiting shapes after sufficient annealing had occurred.

TABLE I. Samples prepared via ion implantation in silica and annealing to study the evolution of chalcogenide nanocrystal size distributions. The last column shows temperatures and annealing times for each sample.

Samples	Implanted species	Energy (keV)	Fluence (atom cm^{-2})	Annealing
PbS1	Pb	510	1.4×10^{15}	800 °C/8 h
	Pb	260	10^{15}	900 °C/8 h
	S	110	1.7×10^{15}	
	S	50	1.3×10^{15}	
PbS2	Pb	500	1.2×10^{15}	900 °C/1 h
	Pb	350	6×10^{14}	
	S	110	2×10^{15}	
PbS3	S	100	2.2×10^{15}	900 °C/4 h
	Pb	480	1.4×10^{15}	
CdSe	Cd	500	1.3×10^{15}	900 °C/1 h
	Se	270	2×10^{15}	

A. Preliminary remark

Our study involves ion-implanted samples, hence a deliberately nonuniform initial solute distribution. Based on the previous section's discussion, we first note that the ion implant fluence plays a major role. For a given implantation energy, high implant fluences F lead to high solute concentrations (typically a few percent in the cases referred to above) and hence to a large chemical potential gradient between the implanted and unimplanted layers. The average solute concentration in a profile of width Δ being

$$\langle c \rangle \approx \frac{F}{\Delta}, \tag{6}$$

growth leads to a family of clusters with average radius $\langle R \rangle$ and average density $\langle n \rangle$ given by

$$\langle n \rangle \approx \frac{3\langle c \rangle}{4\pi \langle R \rangle^3 N_a} \tag{7}$$

where N_a is the atomic density of the cluster phase in the host. Combining Eqs. (5)–(7), the average screening length can be written in terms of the fluence according to

$$\lambda \approx \langle R \rangle \sqrt{\frac{\Delta N_a}{3F}}. \tag{8}$$

With the typical implant profile widths (ca. 100 nm) and fluences (ca. 10^{16} atoms cm^{-2} or more) of the aforementioned experiments, this leads to very small values of λ compared to Δ, and hence to ripening on a very local scale, and to very large heterogeneities in the cluster growth features inside the implant profile—hence to broad (sometimes even bimodal) size distributions. In order to reduce or avoid such effects, we have chosen to perform implants with fluences at or below 10^{16} atoms cm^{-2}. Pb and S were sequentially implanted at 480 and 100 keV, forming PbS nanocrystals ($N_a \approx 19$ PbS nm^{-3}) by annealing at temperature of the order of 800–900 °C. Samples containing 1.24 at. % PbS were

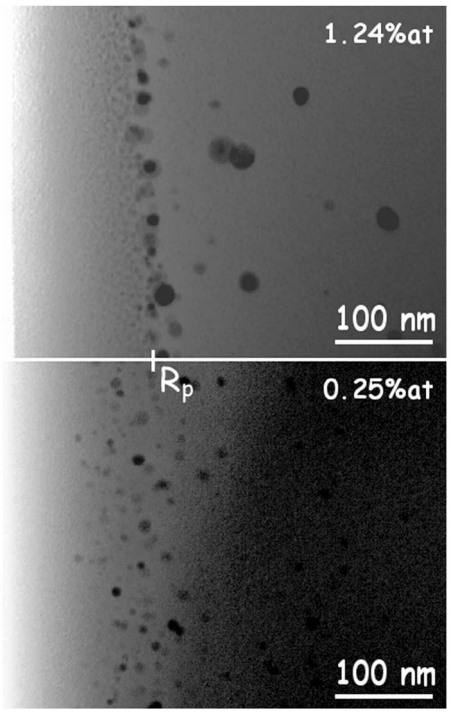

FIG. 1. Illustration of the effect of implant concentration on growth characteristics. Two SiO_2 wafers were sequentially implanted with Pb and S at the same energies, but to different fluences (see text). R_p is the projected range of Pb and S, according to the SRIM code. The 1.24 at. % sample was annealed 1 h at 890 °C and the 0.24 at. % sample was annealed 1 h at 900 °C.

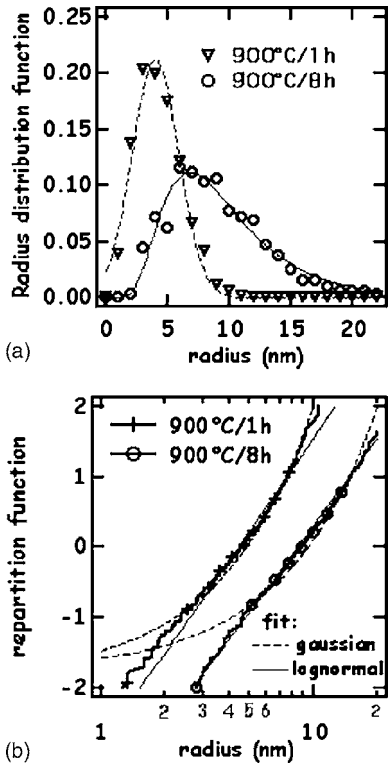

FIG. 2. Experimental radius distribution functions (a) and repartition functions (b) for two samples from PbS1 (Table I) annealed respectively 1 h (inverted triangles) or 8 h (circles) at 900 °C. Full (dashed) lines are lognormal (Gaussian) fits to the data.

synthesized by implanting fluences of 1.1×10^{16} S cm^{-2} and 7×10^{15} Pb cm^{-2}, and samples containing 0.25 at. % PbS by implanting 2.2×10^{15} S cm^{-2} and 1.4×10^{15} Pb cm^{-2}. In the former samples the screening length is very short (about the nanocrystal size), whereas it is comparable to the profile width in the latter, thus leading us to expect significantly more uniform nanocrystal ripening.

This expectation is borne out by transmission electron microscopy observation of the two nanocrystal families after a 1 h anneal at 900 °C (Fig. 1). In the more concentrated samples, very large clusters around the implant concentration maximum testify to very local ripening; and size inhomogeneities and average size variations as a function of depth are significantly larger, in agreement with observations of other solute-host combinations at comparable concentrations.[31,32] All further experiments were performed at concentrations below 0.3 at. %. A series of pure silica plates containing chalcogenide nanocrystals was synthesized by ion implantation of group VI and IV elements. The plates were then each cut up to produce identical samples, which were annealed at different temperatures for different times (Table I) and studied via TEM to deduce their depth and size distributions (see Appendix). More information on the experimental procedure and analysis is given elsewhere.[6,33]

B. When does a size distribution become lognormal?

Figure 2(a) compares the nanocrystal size distributions for identical samples from batch PbS1, annealed at 900 °C for 1 and 8 h, respectively. A 1 h anneal produces a symmetrical Gaussian size distribution around an average radius $R=4.8$ nm, with a standard deviation 1.85 nm (hatched line), whereas the 8 h anneal leads to an asymmetrical distribution, weighted toward larger sizes, that is well fitted to a lognormal (full line). The first two moments (average μ and geometrical standard deviation σ) of the quantity "ln R" are the fitting parameters of the nanocrystal radii data to the lognormal distribution: we find $\mu=8.65$ nm and $\sigma\approx1.5$. An accurate way of judging the quality of fit to a lognormal distribution is to enhance the influence of the distribution tails (i.e., higher-order moments) by plotting the repartition function of the radius distribution in Gaussian coordinates.[34] The repartition function of a lognormal distribution reads

$$F_{\text{lognormal}}(R<r)=\frac{1}{2}\left[1+\text{erf}\left(\frac{\ln r/\mu}{\ln\sigma}\right)\right]. \tag{9}$$

Therefore, plotting $\text{erf}^{-1}[2F_{\text{lognormal}}(r)-1]$ as a function of $\ln(r)$ (principal of Gaussian coordinate) gives a straight line whose slope is a simple function of the geometrical standard deviation only. In such a plot, the experimental repartition function is traced by attributing a weight $1/N$ to each measurement of R, where N is the total number of observed nanocrystals. In Fig. 2(b), we have plotted the results of Fig. 2(a) in this way: the 8 h anneal data provide an excellent fit to a straight line with $\sigma=1.47$ (the 1 h anneal data are shown in the same representation for comparison purposes). Several

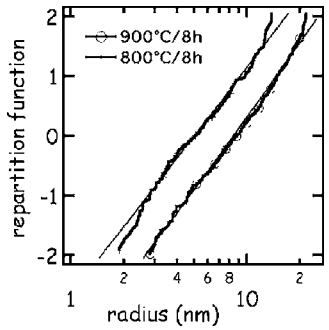

FIG. 3. Influence of annealing temperature on radius repartition function of nanocrystals from PbS1 sample grown at two different temperatures (Table I). Full lines are lognormal fits to the data.

hundred nanocrystals were measured in each run, so that our uncertainty on the geometrical standard deviation is between 2% and 4%. We have thus shown that the size distribution tends to become lognormal when the annealing time increases at a given temperature. As shown in Fig. 3, the same trend occurs when annealing temperature is sufficiently high: the geometrical average of the radius distribution differs, but the shape and geometrical standard deviation are essentially the same.

More generally, obtaining lognormal size distributions was the rule rather than an exception after long-term or high-temperature annealing, including when the implantation profile widths of Pb and S differed or when the implantation sequence was reversed to modify the chemical interaction of the different species with the host.[6] We also observed nanocrystals size distribution of lognormal shape after sequential implantation synthesis of CdSe nanocrystals (see Table I for implantation parameters and thermal treatment). By normalizing all our radius distributions by their geometrical standard deviation, which is found to be in the range 1.45–1.55 in all cases, we may display the compendium of our results as shown in Fig. 4: the equation of the full line (σ=1.5) is

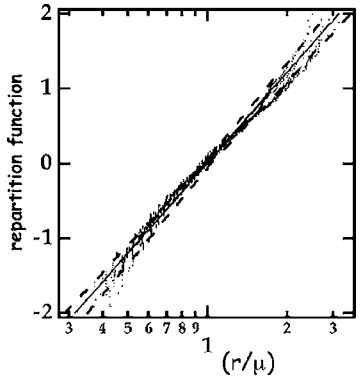

FIG. 4. Radius repartition function (dots) of different samples: PbS1 (μ=5.7 nm) annealed 8 h at 800 °C or (μ=8.7 nm) annealed 8 h at 900 °C; PbS2 (μ=3.2 nm); PbS3 (μ=4.7 nm) annealed 1 h at 900 °C; CdSe (μ=5.0 nm) annealed 1 h at 900 °C. Radii were normalized by the geometrical average radius. Full line, lognormal (geometrical standard deviation 1.5). Dashed lines show the 95% confidence level for the lognormal fit (population 300 precipitates).

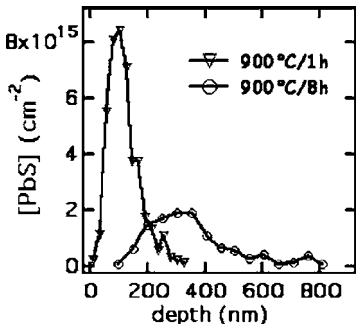

FIG. 5. Comparison (from TEM identification of nanocrystals) of PbS concentration depth dependence for samples from PbS1 after annealing at 900 °C for 1 or 8 h.

$$f_{\text{lognormal}}(z) = \frac{1}{z\ln(1.5)\sqrt{2\pi}}\exp\left(-\frac{[\ln(z)]^2}{2[\ln(1.5)]^2}\right). \quad (10)$$

It is time independent, so that we have an asymptotic distribution; the time dependence is restricted to the geometrical average of the radius distribution, i.e., to the value of μ.

C. How does a size distribution become lognormal?

So far, although our results were obtained by TEM we have plotted the entire size distributions in our figures, regardless of the nanocrystals' depth in the sample. But in inhomogeneous distributions such as these (see Sec. II and Fig. 1), studies of the size distribution cannot be dissociated from a study of the nanocrystal depth dependence. As in our previous work,[29,31] we found that long-term or high-temperature anneals also produced major changes in the nanocrystal depth distributions. A striking example is given in Fig. 5, which presents the depth distributions for the two samples whose size distributions are shown in Fig. 2, as measured by TEM. Whereas the 1 h anneal at 900 °C leads to cluster nucleation and growth inside the implantation profile limits (≈70–250 nm), and to a Gaussian size distribution, the 8 h annealed sample displays a very broad nanocrystal distribution (up to ≈800 nm) and the lognormal size distribution. According to Sec. II annealing leads to an increase in λ in the initially inhomogeneous system, which becomes sensitive to the large chemical potential gradient at the implantation profile edges; nanocrystals then may dissolve in these regions, entailing solute migration. In the case of PbS preferential nucleation and growth of new nanocrystals occurs first at depths corresponding to the implantation profile edges, then at the successive locations of the maximum chemical potential gradient outside of the initial matter concentration profile. Contrary to the process described by LSW, matter is thus not conserved locally, but is transferred progressively outside of the implantation profile.[26] Moreover, nucleation and growth occur during the intervening diffusion. These multiple, interfering mechanisms lead to a complex evolution that bears no direct relation to any single process.

Sufficiently long (or high-temperature) annealing thus blurs the system's memory of its initial nanocrystal synthesis process. This may—and does in our case—occur in other

ways, notably due to the fact that the chemical interaction of chalcogens with silica and group VI elements is complex.[35] This is shown by a study of nanocrystal size distributions obtained from pure silica sequentially implanted with Pb and a chalcogen, annealed in the same temperature range as previously. Data was taken from the very same TEM samples, in which we separated the size distribution corresponding to nanocrystals inside the central part of the implantation profile from that corresponding to nanocrystals outside of the latter. For samples from Table I that were annealed at sufficiently high temperatures or long times, all distributions were lognormal with $\sigma \approx 1.5$. By contrast, we studied nanocrystal size distributions from pure silica sequentially implanted with Pb and Te, annealed 1 h at 890 °C (as noted previously,[35] Te chemistry in silica is probably simpler). The data in Fig. 6 are again taken from the very same TEM sample, after separating the size distribution corresponding to nanocrystals inside the central part of the implantation profile (average radius 4.4 nm) from the size distribution corresponding to nanocrystals outside of the latter (average radius 3.8 nm). The former is obviously complex, reflecting (but not completely erasing) the competing nucleation mechanisms due to Te chemistry; while the latter is practically lognormal, with a geometrical standard deviation of 1.5 as above. The memory loss of initial conditions inside the implantation profile is not as complete for Te as for the other chalcogens, but the additional effects of cluster dissolution, solute diffusion and clustering again lead to the lognormal size distribution.

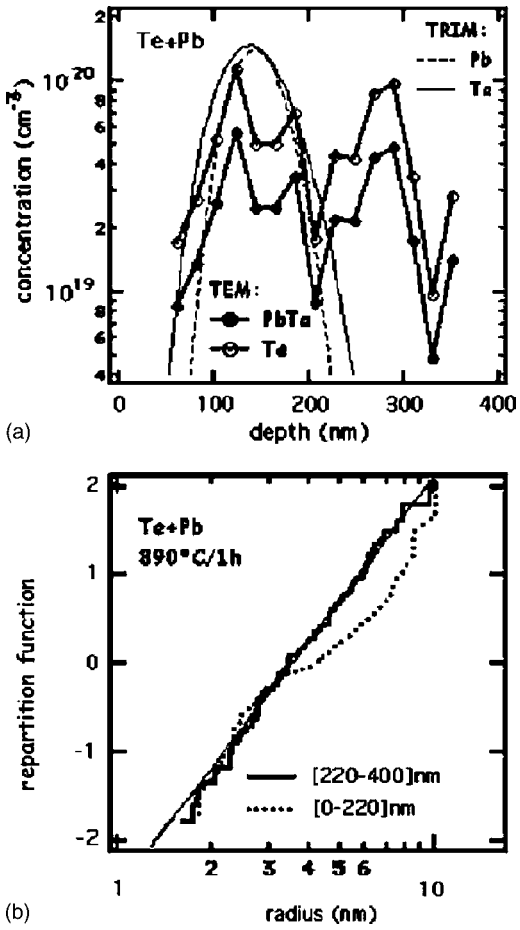

FIG. 6. (a) Comparison of initial concentration profiles of Pb and Te as determined by SRIM (thin lines, full and dashed) with precipitated element concentration as measured by TEM, assuming that all the precipitates are either PbTe (full dots) or Te (circles). Sample is Te+Pb sequentially implanted silica annealed 1 h at 890 °C. (b) Size repartition function in Gaussian coordinates as a function of depth in the Te+Pb sequentially implanted silica sample, after annealing 1 h at 890 °C. Two depth ranges were analyzed separately: 0–220 nm corresponds to the implanted profile (dotted line), and the other to greater depths (full line). Thin straight line, lognormal fit to nanocrystal radius repartition function for depths greater than 220 nm ($\sigma = 1.4$).

IV. DISCUSSION

The existence of an asymptotic form of the nanocrystal size distribution after long-term annealing is a well-known property of relaxing systems; it is also well-known that the detailed shape of such a distribution depends on the microscopic growth mechanism. Binder's presentation[17] of the asymptotic behavior emphasized the analogy of the ripening treatment in the two very different growth regimes—that of condensation and that leading to coagulation. He derived an equation describing the size distribution evolution assuming growth by condensation and coagulation. The evolution of the number of clusters of size l may be rewritten in the following schematic way:

$$\left.\frac{\partial n_l}{\partial t}\right|_{\text{tot}} = \nabla \vec{J} + \left.\frac{\partial n_l}{\partial t}\right|_{\text{coag}}. \tag{11}$$

The first term describes precipitation by condensation by monomers and very small clusters, where $\vec{J}$ is the current of clusters in size space. The second term describes precipitation by coagulation in way analogous to Eq. (4). Binder shows how that the search for the asymptotic behavior is analogous in both growth regimes. One searches for a size distribution of the form

$$n_l(t) = t^y \tilde{n}(lt^{-x}) \quad t \to \infty, \tag{12}$$

where x and y are time exponents to be determined with the help of Eq. (11) and the mass conservation equation

$$\frac{d}{dt}\int_0^\infty n_l(t) l \, dl = 0. \tag{13}$$

Mass conservation thus leads to $y = -2x$, whether growth occurs by coagulation or condensation. The specific growth mechanisms only enter into account by taking either the first or the last term in Eq. (11). In the case of condensation driven by the surface tension effect (Gibbs-Thompson equation), one obtains an analytic equation which leads to the LSW form for $\tilde{n}$ and $x = 1/3$. In accordance with the LSW result, normalizing by the mean size allows one to write the size distribution as in Eq. (12). For coagulation, the equation verified by $\tilde{n}$ is nonlinear and difficult to handle, but its solution has been shown[19–21] to approximate a lognormal one when $t \to \infty$.

In the classical LSW description of ripening, there is a direct relation between the initial nanocrystal population, its spatial distribution and the precipitate size evolution. No nucleation occurs during ripening, and solute atoms travel between existing clusters. The clusters who have survived long term anneals were present in the initial stages of the ripening process. We have shown that in our implanted samples, after sufficient annealing (Figs. 2 and 3) the nanocrystal population and its spatial distribution bear no relation at all to the initial distribution. Therefore, the LSW ripening description does not apply at all to the present case. In other words, after ripening a homogeneous system conserves memory of its initial structure and may lead to the LSW size distribution, whereas in our inhomogeneous samples the memory is entirely lost, leading to a lognormal distribution. This relation between our results and a loss of information may be quantified as follows.

It is well known[36] that the amount of information contained in some distribution f may be evaluated by calculating its entropy:

$$S = -\int f \ln f. \tag{14}$$

Jaynes[37] showed that this applies to statistical physics: e.g., entropy is maximized at equilibrium, as expected from basic thermodynamics. It also applies to growth statistics, as discussed by Wang and Friedlander[38] who emphasized the similarity between asymptotic growth distributions and limiting values in the kinetic theory of gases. Rosen[39] first applied the entropy maximization principle to coagulation. Conservation equations [matter conservation via Eq. (13) and size space population conservation via Eq. (11)] provide constraints to be satisfied during the maximization procedure. In other words, the agreement between the experimental and the calculated size distribution depends on the amount of information supplied by the constraints. Under very general constraints on volume conservation, Rosen finds an asymptotic form

$$\tilde{n}(u) = \exp(-u) \tag{15}$$

where u is the normalized volume. It is a very good approximation to the lognormal distribution found by Friedlander, in the large-size limit ($u > 1$), whereas other constraints such as the evolution equation are needed in the small size regime.

May we reason in the same way as regards condensation? The results of Sec. III show that as major constraints on the nucleation and growth process are relaxed, the limiting shape of the size distribution becomes lognormal. This is summarized in Fig. 7, in which we compare our results to Eq. (15): excellent agreement is found, except for the smallest sizes where some reminiscence of the initial growth process remains. This is a strong indication that the discussion given above for coagulation may also be applied to condensation.

In order to obtain other distribution shapes—e.g., the LSW shape in the case of binary alloys—further constraints are required, such as that introduced by the Gibbs-Thomson surface tension criterion leading to LSW. Since the LSW picture fails in our system (Sec. III), the volume conservation constraint alone is sufficient to approach the experimental distributions.

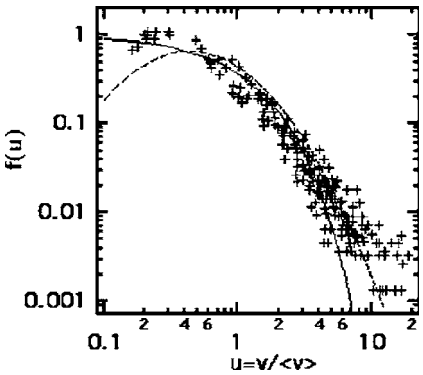

FIG. 7. Reduced volume (u) probability density plot. Crosses are experimental data for various semiconductor (PbS, PbSe, CdSe, PbTe) nanocrystals grown after sequential implantation of the components into pure silica (fluences ca. 10^{15} atoms cm^{-2}) at energies in the 100–300 keV range, and annealing in the range 800–900 °C for several hours. The full line is the maximum entropy distribution e^{-u}, determined by the sole constraint of volume conservation; the dashed line is the best fit of experimental data ($u > 1$) to the reduced lognormal distribution ($\mu = 1$).

The constant value of the geometrical standard deviation of about 1.5 that we observed in our experiments was also found in aggregation studies by Gmachowski.[8] Assuming a lognormal shape, he performed entropy maximization calculations of the most probable geometrical standard deviation that all led to values between 1.40 and 1.54, in spite of the broad variety of aggregate shapes and aggregation processes considered by him. The spread is rather narrow and the values are close to ours, again indicating that very little information may be deduced on the growth process from such size distribution shapes.

V. CONCLUSION

A general scheme of nanocrystal growth, at a given temperature, in a nonuniform concentration (e.g., implantation) profile may thus be described in the following way. As long as the slowest species remains inside the implantation profile, the shape of the size distribution is determined by the growth history (detailed nucleation conditions, diffusion, and reaction between species). In the homogeneous concentration case, diffusing solutes move upon annealing into regions where precipitates have already formed, and participate in Ostwald ripening leading to the LSW size distribution. When ion implantation is involved, the situation diverges from this picture because solutes out-diffusing from the implanted profile travel to a precipitate-free region where random nucleation screens the effect of surface tension, and leads to a lognormal shape with a geometrical standard deviation around 1.5. Alternatively, complex chemical reactions may produce the same result. The nucleation and growth history of the clusters is no longer revealed by the distribution shape: it is only contained in the geometrical average radius.

The lognormal distribution is only due to very general constraints on the system's evolution, such as matter conservation. Finally, we note that the lognormal shape is only a convenient approximation of the real size distribution, which may be approximated by other analytical forms.

In the case of narrow concentration profiles, nanocrystal size distribution control will only be possible for average sizes limited to a few nanometers; because they tend to provide a more uniform initial matter distribution, multienergy implants allow control over a greater size range, as found empirically in past experiments.

ACKNOWLEDGMENTS

We are very grateful to K. H. Heinig for critical discussions, and to O. Kaitasov and S. Collin for technical assistance.

APPENDIX: A PROCEDURE TO DETERMINE NANOCRYSTAL DENSITIES AND SIZE DISTRIBUTIONS

In order to determine the nanocrystal depth and size distributions from TEM images, we set up a procedure to minimize bias in the determination of the nanocrystal radii and integrated matter depth dependences. Since we deal with samples involving inhomogeneous solute concentrations, nucleation does not occur uniformly in depth. Hence, special care was taken to acquire images of TEM cross sections in which the SiO_2 or glass surface was parallel to one side of the frame. As TEM samples usually do not have a uniform thickness, the background gray level in the corresponding images show variations that can bias the nanocluster radius measurement, depending on the nanocrystals' position in the layer. To obviate this problem, we first applied a Sobel-type gradient operator to all frames before measuring the nanocrystals' size and position. The nanocrystal density was such that there were no overlapping nanocrystal images at typical sample thicknesses. Hence, all nanocrystal radii, depth and precipitated matter concentrations could be compiled. On a TEM micrograph, only a surface density of nanocrystals (i.e., surface concentration projected on the image plane along the electron beam direction) is measured. The thickness of the cross-section sample, unless specified otherwise, was taken to be 100 nm. In order to determine the precipitated matter concentration, the nanocrystal volumes (deduced from their radius) were summed in a given depth slice, and then divided by the average TEM cross-section thickness and the number of crystalline units per volume (19.1 PbS nm^{-3}; 14.9 PbTe nm^{-3}).

*Corresponding author. Electronic address: bernas@csnsm.in2p3.fr

[1] S. V. Gaponenko, *Optical Properties of Semiconductor Nanocrystals* (Cambridge University Press, Cambridge, U.K., 1998).
[2] B. O. Dabbousi, J. Rodriguez-Viejo, F. V. Mikulec, J. R. Heine, H. Mattoussi, R. Ober, K. F. Jensen, and M. G. Bawendi, J. Phys. Chem. B **101**, 9463 (1997).
[3] A. Sashchiuk, E. Lifshitz, R. Reisfeld, T. Saraidarov, M. Zelner, and A. Willenz, J. Sol-Gel Sci. Technol. **24**, 31 (2002).
[4] I. M. Lifshitz and V. V. Slyosov, J. Phys. Chem. Solids **28**, 35 (1961).
[5] C. Wagner, Z. Elektrochem. **65**, 58 (1961).
[6] R. Espiau de Lamaestre, J. Majimel, F. Jomard, and H. Bernas, J. Phys. Chem. B **109**, 19148 (2005).
[7] E. Limpert, W. A. Stahel, and M. Abbt, BioScience **51**, 341 (2001) and references therein; see http://www.inf.ethz.ch/personal/gut/lognormal/.
[8] L. Gmachowski, Colloids Surf., A **176**, 151 (2001); **201**, 41 (2002).
[9] C. S. Graham and A. J. Robinson, J. Aerosol Sci. **7**, 261 (1976).
[10] S. Yatsuya, S. Kasukabe, and R. Uyeda, Jpn. J. Appl. Phys. **12**, 1675 (1973).
[11] C. G. Granqvist and R. A. Buhrman, J. Appl. Phys. **47**, 2200 (1976).
[12] A. Miotello, G. De Marchi, G. Mattei, P. Mazzoldi, and C. Sada, Phys. Rev. B **63**, 075409 (2001).
[13] E. Borsella, M. A. Garcia, G. Mattei, C. Maurizio, P. Mazzoldi, E. Cattaruzza, F. Gonella, G. Battaglin, A. Quaranta, and F. D'Acapito, J. Appl. Phys. **90**, 4467 (2001).
[14] H. H. Andersen and E. Johnson, Nucl. Instrum. Methods Phys. Res. B **106**, 480 (1995).
[15] S. Hagège and U. Dahmen, Philos. Mag. Lett. **74**, 259 (1996), and reference therein.
[16] E. Valentin, H. Bernas, C. Ricolleau, and F. Creuzet, Phys. Rev. Lett. **86**, 99 (2001); E. Valentin, Ph.D thesis, Ecole Centrale de Paris, 1999.
[17] K. Binder, Phys. Rev. B **15**, 4425 (1977).
[18] M. von Smoluchowski, Phys. Z. **17**, 585 (1916).
[19] S. K. Friedlander and C. S. Wang, J. Colloid Interface Sci. **22**, 126 (1966).
[20] D. L. Swift and S. K. Friedlander, J. Colloid Sci. **19**, 621 (1964).
[21] G. M. Hidy, J. Colloid Sci. **20**, 123 (1965).
[22] P. T. Spicer and S. E. Pratsinis, Water Res. **30**, 1049 (1996).
[23] C. S. Graham and A. J. Robinson, J. Aerosol Sci. **7**, 261 (1976).
[24] R. Jullien, New J. Chem. **14**, 239 (1990).
[25] J. Söderlund, L. B. Kiss, G. A. Niklasson, and C. G. Granqvist, Phys. Rev. Lett. **80**, 2386 (1998).
[26] H. Trinkaus and S. Mantl, Nucl. Instrum. Methods Phys. Res. B **80/81**, 862 (1993).
[27] V. A. Borodin, Physica A **211**, 279 (1994).
[28] V. A. Borodin, K. H. Heinig, and S. Reiss, Phys. Rev. B **56**, 5332 (1997).
[29] R. Espiau de Lamaestre and H. Bernas, J. Appl. Phys. **98**, 104310 (2005).
[30] R. Espiau de Lamaestre, H. Bernas, and F. Jomard, Nucl. Instrum. Methods Phys. Res. B **216**, 402 (2004).
[31] A. Meldrum, E. Sonder, R. A. Zuhr, I. M. Anderson, J. D. Budai, C. W. White, L. A. Boatner, and D. O. Henderson, J. Mater. Sci. **14**, 4489 (1999).
[32] C. Bonafos, B. Garrido, M. Lopez, A. Romano-Rodriguez, O. Gonzales-Varona, A. Perez-Rodriguez, and J. R. Morante, Appl.

Phys. Lett. **72**, 3488 (1998).
[33] R. Espiau de Lamaestre, Ph.D. thesis, University Paris XI, 2005.
[34] N. L. Johnson and S. Kotz, *Distributions in Statistics—Continuous Univariate Distributions* (John Wiley & Sons, New York, 1970), Vol. 1, pp. 112—136.
[35] R. Espiau de Lamaestre, F. Jomard, J. Majimel, and H. Bernas, J. Non-Cryst. Solids **351**, 3031 (2005).
[36] C. E. Shannon, Bell Syst. Tech. J. **27**, 379 (1948); **27**, 623 (1948).
[37] E. T. Jaynes, Phys. Rev. **106**, 620 (1957); **108**, 171 (1957).
[38] S. K. Friedlander and C. S. Wang, J. Colloid Interface Sci. **24**, 170 (1967).
[39] J. M. Rosen, J. Colloid Interface Sci. **99**, 9 (1984).